Simulation study of structural changes in zeolite RHO

S. R. G. Balestra,[1] J. J. Gutiérrez–Sevillano,[1] P. J. Merkling,[1] D. Dubbeldam,[2] and S. Calero[1,*]

[1] *Department of Physical, Chemical, and Natural Systems, University Pablo de Olavide, Ctra. Utrera km 1, 41013 Seville, Spain*

[2] *Van 't Hoff Institute for Molecular Sciences, University of Amsterdam, Science Park 904, 1098XH Amsterdam, The Netherlands*

Flexibility in zeolite RHO manifests itself in its ability to adopt one of two structures, depending on the composition and the applied external conditions. In this work, structural changes of dehydrated zeolite RHO of composition $(Na_6Cs_3)O_{96}Al_9Si_{39}$ and pure silica were investigated by molecular dynamics (MD) and Monte Carlo methods using the force field by Nicholas et al. (*J. Am. Chem. Soc.* **1991**, 113, 4792). The structure was found, depending on temperature, to be stable in the acentric form (space group $I\bar{4}3m$) below ∼300 K and in the centric form ($Im\bar{3}m$) above, in qualitative agreement with experimental findings from the literature. Additionally, the structure may remain in the centric form in metastable conditions at all temperatures and exhibits a negative thermal expansion (NTE) of $-(13\pm3)\times10^{-6}$ K^{-1}. Calculated X-ray diffraction patterns match the experimental ones closely confirming the assignments to space groups made on the basis of lattice sizes. Modifications on the force field were investigated and other established force fields probed. A detailed knowledge and control over the behaviour of this structure should lead to more reliable predictions on applications like separation of gases.

Graphical TOC Entry:

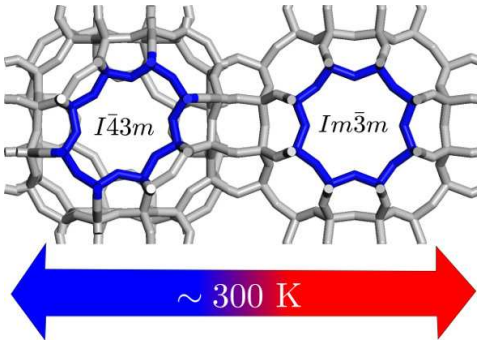

Keywords: zeolite, RHO, flexibility, phase transition

* scalero@upo.es

I. INTRODUCTION

Zeolites are crystalline aluminosilicate materials that possess intra-crystalline voids of molecular dimensions. All of the frameworks they form are known to show small deformations, although some structures are particularly flexible [1]. Amongst these, zeolite RHO exhibits unique structural changes. Depending on the conditions, it has been shown to appear in one of two cubic space groups, a centric $Im\bar{3}m$ form or an acentric $I\bar{4}3m$ form, as shown in Figure 1. Factors that affect the preferred form include the nature of the cations [2], amount of hydration [3], temperature [4] and pressure [5]. This high sensitivity to the conditions and composition of this zeolite makes it an excellent candidate for a theoretical study modelling it as a flexible framework.

The RHO topology is composed of α-cages linked *via* double 8-rings. The double 8-rings are deformable and have a degree of ellipticity or distortion as shown in Figure 1. It is quantified by a parameter Δ as defined by Parise et al.:[6]

$$\Delta_{ijkl} = \frac{1}{2}\|r_{ij} - r_{kl}\| \tag{1}$$

where $r_{ij} = |\vec{r_i} - \vec{r_j}|$ and i, j, k, l are defined in Figure 1. The distortions in double 8-rings are accompanied by a large change in unit cell length a [4].

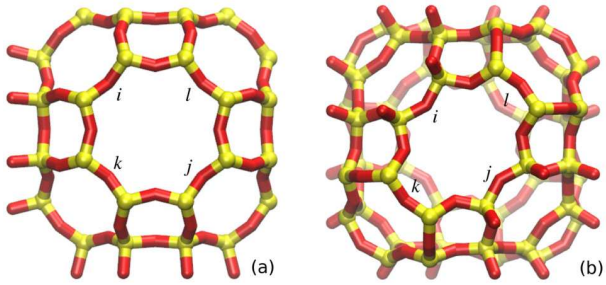

FIG. 1. Zeolite RHO (a) $Im\bar{3}m$ space group with $a \sim 15.0$ Å, (b) $I\bar{4}3m$ space group with $a \sim 14.6$ Å.

The flexibility of this zeolite has been extensively studied in the past. However, to the best of our knowledge, this aspect has not been studied by simulation previously. The aim of this work is to study zeolite RHO of an ideal composition at low pressure using flexible force fields. The success of predictions critically depends on the force fields chosen. Several of them have been previously reported and found wide use in the area of flexible zeolites, such as the model of Nicholas et al.[7], Hill and Sauer [8, 9], Demontis et al.[10] and a core–shell model of Schröder and Sauer [11]. A recent simulation study supports Nicholas' model as the one that performs better in infrared studies than other force fields investigated [12]. Unless indicated otherwise, this is the default force field used in this work.

Another recent experimental study reports high selectivity of zeolite RHO for CO_2 in CO_2/CH_4 separations. The authors find that the partial pressure of CO_2 causes a change in structure and hypothesize that the phenomenon is induced by interactions between the flexible framework and the CO_2 in the proximities of the window [13]. Understanding this phenomenon may lead to interesting contributions to environmental technology and the capture of greenhouse gases, but before that it is necessary to gain a better, more fundamental understanding of the flexibility of zeolite RHO.

II. SIMULATION METHODS

Zeolitic frameworks are treated as periodic networks based on periodic boundary conditions (PBC). This crystalline tessellation —the framework— is performed from the simulation box by endless Euclidean translations in all three spatial directions. The interactions between particles are calculated according to the force field chosen. Unless specified otherwise, this is the force field by Nicholas et al.[7]. Electrostatic energy of a crystalline system is conditionally convergent. To avoid infinities, Ewald summation was used. The cut off radius for short-range interactions was set to 12 Å.

The crystal is considered vacuous and in vacuum. To make the structures ($Im\bar{3}m$ and $I\bar{4}3m$ forms) we have used the atomic coordinates provided by the crystallographic study of Palomino et al.[13].

To calculate micro-states compatible with environmental conditions (constant particle number, volume, and temperature) canonical Monte Carlo (abbreviated MC NVT) was used. Isothermal-isobaric ensemble (constant particle number, pressure, and temperature, abbreviated NPT) molecular dynamics (MD) was used to study the evolution of the system. The method used to equilibrate is the Parrinello–Rahman barostat[14]. The Martyna et al. algorithm [15] is used for velocity Verlet integrators —validated by Tuckerman et al.[16, 17]—. When we keep fixed the pressure, it is equal to 1 mTorr —an experimental vacuum—. Simulations were run for 100-1000 ps using an integration time step of $\tau = 5 \times 10^{-4}$ ps.

Energy minimizations have been calculated at fixed volume using the Baker method.[18]

Since the space groups involved in this study are cubic but cell lengths in the simulations are allowed to evolve independently from each other, the length of the unit cell at temperature T was considered as the time average $a_T = \frac{1}{3}\langle a^t_{xT} + a^t_{yT} + a^t_{zT}\rangle_t$.

III. RESULTS AND DISCUSSION

A first concern that arises when dealing with this structure is the observation that the phase transition $Im\bar{3}m \leftrightarrow I\bar{4}3m$ was observed in zeolite RHO of composition $Na_6Cs_3)O_{96}Al_9Si_{39}$,[13] while a pure silica version has yet to be synthesized. It is therefore important to assess the role of tetrahedral aluminium in enabling this structural change.

Atomic coordinates were taken from Palomino et al.[13] for the $I\bar{4}3m$ form. The aluminium atoms have a non-periodic occupation of lattice sites in the crystalline structure. To model this system, a crystalline configuration is set up in which a random replacement of 9 SiO_4 by 9 AlO_4 tetrahedra is undertaken and bound to obey Lowenstein's rule. Monovalent cations (6 Na^+ and 3 Cs^+) were randomly added to compensate for the charge of the framework. Around $\sim$ 1000 different configurations were generated and MC simulations run on them that yielded as many values for internal energies $\mathcal{U}$. Volume, temperature, and number of atoms were fixed (NVT ensemble) so that the experimental density was reproduced and temperature was set to a low 3 K. Each configuration $k = 1, \ldots, 1000$ is characterized by its average distance between aluminium atoms $\langle \text{Al Al}\rangle_k$ and its internal energy $\mathcal{U}_k$ and represented in Figure 2 (top). Internal energies were computed because of their independence from pressure so the simulations were expected to be a bit more robust. However, they compare favourably with simulations in the isothermal-isobaric ensemble. Under these conditions of low temperature, the internal energy $\mathcal{U}$ is almost equal to the free energy $\mathcal{F}$ and therefore the internal energy serves as a measure of the stability of the framework. If each configuration k is in equilibrium at temperature T, it can be assigned a weighting factor $P_k \propto \exp(-\mathcal{U}_k/k_BT)$. In Figure 2, the obtained probability density is depicted in a histogram. The distance *vs* internal energy data on the other side scatter strongly. A line corresponding to a linear fit was laid through the simulation data and showed a correlation that is essentially within the error bars. The correlation coefficient is $r^2 \simeq 0.035$.

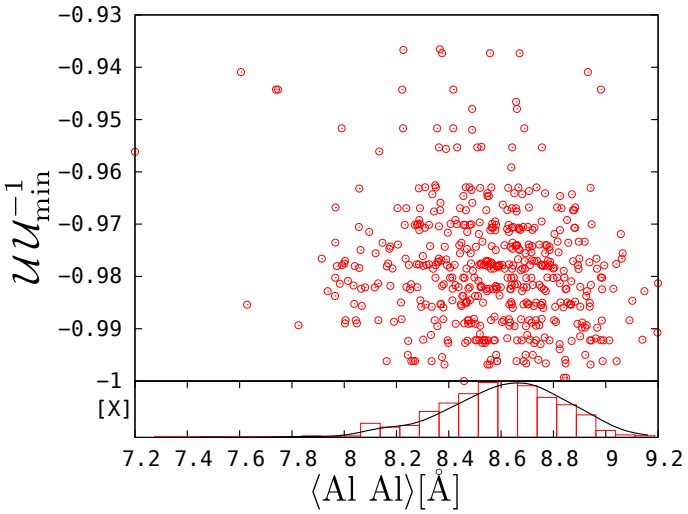

FIG. 2. Top: Dimensionless internal energy $\mathcal{U}\,\mathcal{U}^{-1}_{\rm min}$ (with $\mathcal{U}^{-1}_{\rm min} \simeq 6.4k_B \times 10^6$ K, absolute value of the configuration with lowest energy) *versus* average distance between Al atoms in randomly generated RHO frameworks. The dashed line represents a linear fit through the data. Bottom: Probability density as a function of average distance between aluminium atoms. The dashed line represents a normal distribution fit.

Any configurations of $SiO_4 \rightarrow AlO_4$ replacements in presence of monovalent cations is valid as long Lowenstein's rule is fulfilled. Since, the aluminium distribution does not seem to be the primary cause of the structural changes of ideal flexible zeolite RHO, and to gain simplicity it will assumed that the role of aluminium should not be critical for the observation of structural changes. From now on, only the hypothetical pure silica zeolite RHO will be considered.

A. Temperature effect

Changes in temperature affect the volume in two ways: on the one hand, the structural change between space groups $Im\bar{3}m$ and $I\bar{4}3m$, and on the other hand, the dependence of unit cell volume on temperature within the same space group. By use of neutron diffraction and X-ray diffraction, Parise et al.[4] observed a gradual increase in unit cell volume upon heating from 11 to 573 K, together with a decrease in the geometrical parameter Δ that is defined in Equation 1. Their results led them to conclude that upon heating, the structure changes progressively from $I\bar{4}3m$ to $Im\bar{3}m$ and estimated by extrapolation that this process would complete at 800 K. In the current work, the temperature effect was studied by molecular dynamics in the NPT ensemble under conditions described in the Methods Section. The length of unit cell a was computed and attention paid to its evolution during simulation. The temporal evolution of the length of the unit cell for temperatures 11, 295 and 423 K is shown in Figure 3 (left). The system in these early stages of the simulation is obviously outside of thermodynamic equilibrium conditions, and was started with the experimental 11 K cell parameters and $I\bar{4}3m$ space group. It is striking how fast the equilibrium value of the cell parameter is reached, even at a nominal 11 K. The space group on the other side was stable in the simulations at 11 and 295 K, but switched to the high-symmetry $Im\bar{3}m$ form at 423 K within a picosecond of simulated time. The average values $a_T = \langle a_T^t \rangle_t$ achieved above 10 ps can be represented in a systematic way versus temperature T, as shown in Figure 3 (right) when simulations are investigated using both the $Im\bar{3}m$ and $I\bar{4}3m$ initial conditions. As can be seen from this figure, at 423 K and 800 K frameworks adopt the high-symmetry form. At 300 K and below on the other side, the frameworks retained their symmetry over the duration of the simulations. One of the interesting consequences is that it is possible to follow the evolution of the volume of the high-symmetry structure over the whole range of temperatures in these simulations. A linear regression of the a_T values of structures that retain the centric form yields

$$a_T \simeq a_0 + T \left(\frac{\partial a}{\partial T} \right)_P \tag{2}$$

where $a_0 = 14.012$Å and $(\partial a/\partial T)_P = -(6 \pm 1)10^{-5}$Å with $r^2 \simeq 0.75$. Thus, an intrinsic negative thermal expansion (NTE) was observed with a coefficient of thermal expansion α_V of $\frac{3}{a}\left(\frac{\partial a}{\partial T}\right)_P = -(13 \pm 3) \times 10^{-6}$ K^{-1}. This value is consistent with the results given by Miller et al.[19] It can be noted also that while transitions from the acentric to the centric form have been observed, no transition took place from the centric to the acentric form.

While in the case of zeolite RHO the overwhelming effect of the structural change $Im\bar{3}m \leftrightarrow I\bar{4}3m$ on the unit cell length a prevents an experimental confirmation of the phenomenon of NTE, the results from the simulations are consistent with the behaviour of zeolites with LTA topology where similar, although slightly bigger NTE values were reported by Carey et al.[20] Although it has been taken so far for granted that big changes in unit cell lengths are associated with a change in structure, these can be probed in a more authoritative way by calculating powder X-ray diffraction patterns and comparing them to available experimental data. Given that there is a significant difference in average cell lengths between simulations and experiments and according to Bragg's law this would lead to a shift in 2θ values, the simulation cells were rescaled. Using this approach, the identification of the symmetry is made easier and less ambiguous. The results for a CuK_α radiation (λ = 1.5418 Å) are shown in Figure 4 and compared with experimental data from Palomino et al.[13] Changes in the diffraction patterns are most prominent in the $23^\circ < 2\theta \leq 29^\circ$ region. The identification of the framework symmetry of the simulations that were shown in Figure 3 (left) is confirmed by the representations in Figure 4. Clearly, the data for the simulation at 11 K agree well with experimental $I\bar{4}3m$ data. It can be concluded that the simulation maintains the lower-symmetry form it started with, while simulations at 295 and 423 K both are found to belong to the high-symmetry form. The simulation at 423 K is especially interesting because it is the only one of the three simulations shown that was started with $I\bar{4}3m$ symmetry but was converted to $Im\bar{3}m$. In Figure 4, the unit cells had been rescaled to the corresponding experimental values, as has been stated previously. One might check that the XRD calculated does indeed contain new structural information that enables the identification. To this end, the XRD pattern was recalculated using the cell lengths of the *other* space group (Supporting Information). As a result, it is found that now the low-symmetry form is rather similar to the experimental high-symmetry form, and vice versa. So the cell lengths are clearly very important. However, the peak at 28-29° in $I\bar{4}3m$ is missing when the real cell length, but the wrong symmetry is used.

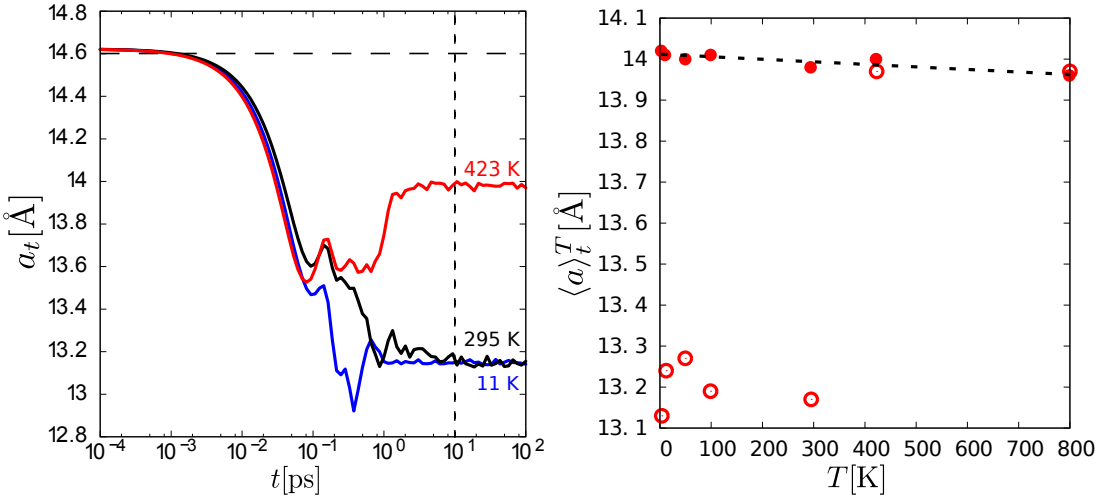

FIG. 3. Left: length of unit cell a^t *versus* time t at 11 K (blue), 295 K (black) and 423 K (red). The dashed lines marks (horizontal) the experimental length of the unit cell at 11 K, and (vertical) the time in which we start to calculate the mean value. Right: $\langle a_T^t \rangle_t$ *versus* temperature T; the simulations started with $Im\bar{3}m$ (•) and $I\bar{4}3m$ (⊙). The dashed line represents a linear fit to the $Im\bar{3}m$ form.

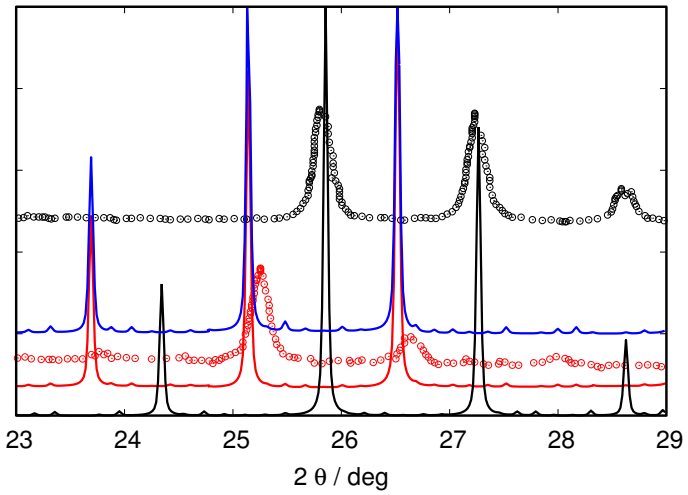

FIG. 4. X-ray diffraction patterns using CuK$_\alpha$ radiation. Red circled dots (⊙) correspond to an experimental determination attributed to space group $Im\bar{3}m$[13] and black circled dots (⊙) to space group $I\bar{4}3m$. Red solid lines correspond to rescaled simulation structures at 11 K, black solid lines to the ones at 11 K, and blue dashed lines to the ones at 423 K. 2θ error bars are smaller than the line widths.

Furthermore, it is also possible to quantify directly the deformation of the structure Δ. The energy of the structure was minimized at constant a. This calculation provides the equilibrium paths (at $T = 0$ K) on the potential energy surface $\mathcal{U} = \mathcal{U}(a, \Delta)$. Two main potential wells were found: one at $\Delta = 0$ and another at $\Delta \neq 0$. Figure 5 shows two sections of the surface. It can be noted that with this force field, $Im\bar{3}m$ is more stable at 0 K although the potential wells allow systems to get trapped in any of them at low enough temperature. The position of the minima is consistent with the calculations using NPT MD depicted in Figure 3. In Figure 5(left), a data point at $\simeq$ 12.7 Å, $u = -0.99$ has a deformation Δ=0 and seems to be an outlier. In fact, this is a significantly deformed window as can be seen in the snapshot obtained by minimization of the $Im\bar{3}m$ form at low volume (Figure 6). It would be interesting to see if this structure can be formed under high pressure conditions (supporting Figure 2). At still lower volumes, the $Im\bar{3}m$ form is converted to the $I\bar{4}3m$ form, an observation in keeping with experimental findings [5].

The model reproduces also nicely the relationship between the amount of deformation Δ in the windows and the cell length that was already observed by Parise and Prince:[6] for example, the structure responds to a 0.7 Å shortening

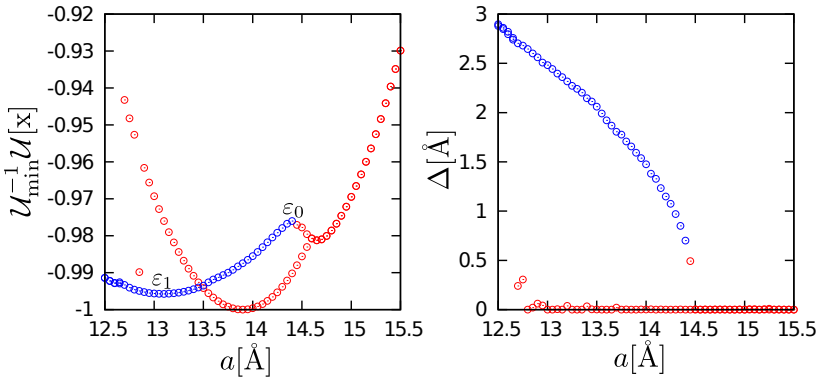

FIG. 5. Equilibrium paths on the potential energy surface at 0 K $u = -\mathcal{U}_{\min}^{-1}\mathcal{U}(a, \Delta)$ with $k_B^{-1}\mathcal{U}_{\min} = -6.77 \times 10^6$ K for Nicholas et al.'s force field. Systems with $\Delta < 0.5$ Å in red and $\Delta \geq 0.5$ Å in blue.

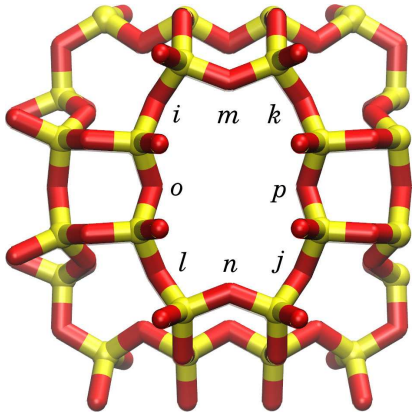

FIG. 6. Minimized structure at low volume belonging to space group $Pm\bar{3}$. $\Delta_{ijkl} = 0$ but $\Delta_{mnop} = 0.92$ Å.

of its unit cell with a deformation $\Delta \approx 1.8$ Å and the downwards curvature is similar to the experimental one.

So far, the model of Nicholas et al. has been used. In the next section, modifications on this model are studied to assess the sensitivity of the properties calculated hitherto on details of the force field. The first parameter modified was the set of partial charges.

B. Effect of charges

Electrostatic interactions are long-ranged and small modifications in charges can lead to relevant effects on the volume of the cell or on its symmetry. In order to assess the sensitivity of the structures on partial charges in the system, two modifications of Nicholas et al.'s[7] force field were tested: a zero-charge model and a model by García–Sánchez et al.[21] This model uses the same intramolecular contributions as Nicholas et al.'s model, but charges and van der Waals contributions have been fitted for a more accurate reproduction of CO_2 adsorption in zeolites. Very roughly speaking, charges are reduced by around 40%. So in comparison with Nicholas et al.'s model, the models considered in this part weaken the electrostatic interactions.

With these new parameters, NPT MD calculations were repeated under the same conditions of pressure and temperatures as in Figure 3 (left). The time averaged values a_T at different temperatures have been added in Figures 7a and 7c for the corresponding model.

Energy minimization calculations of the structure for García–Sánchez et al.'s model and the zero-charge model were performed and are shown in Figure 7.

The simulations revealed that independently of the starting structure and of the model, the framework ended up in the high-symmetry, $\Delta = 0$ structure since this is the lowest energy structure according to these models. How much thermal activation is required for the structure to be converted into the high-symmetry variant can be related

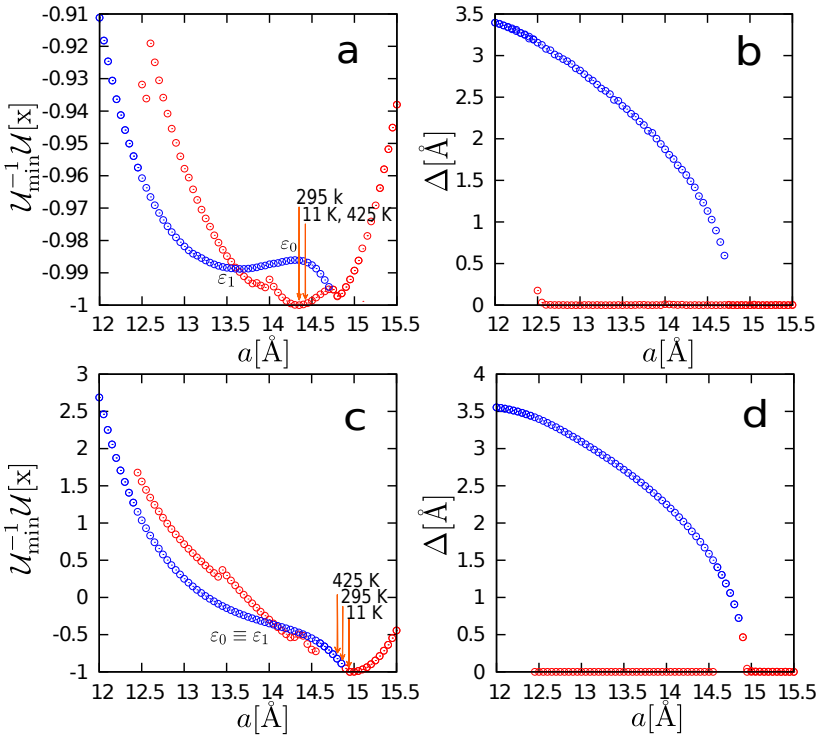

FIG. 7. (a) Equilibrium paths on the potential energy surface $u = \mathcal{U}_{\rm min}^{-1}\mathcal{U}(a, \Delta)$ and (b) Δ-parameter for García–Sánchez et al.'s model, where $k_B^{-1}\mathcal{U}_{\rm min} = 3.46 \times 10^6$ K/ unit cell, and corresponding plots for a zero-charge model (c and d) where $k_B^{-1}\mathcal{U}_{\rm min} = 1.51 \times 10^5$ K/unit cell. Systems with $\Delta < 0.5$ Å in red and $\Delta \geq 0.5$ Å in blue. The orange arrows indicate $\langle a_T^t \rangle_t$ computed by NPT MD.

qualitatively to barrier height $\delta = \varepsilon_0 - \varepsilon_1$. The variables represent the energy ε_0 of the principal barrier and ε_1 of the bottom of the well of $\Delta \geq 0.5$ structures. These variables are marked in Figures 5 and 7. Nicholas et al.'s model predicts a difference of $2\delta k_B^{-1}(3N-6)^{-1} \simeq 633.8$ K, García–Sánchez et al.'s a difference of $2\delta k_B^{-1}(3N-6)^{-1} \simeq 44.3$ K, and the zero-charge model has no energy barrier for $\Delta > 0$.

However, with decreasing point charges, the length of the minimum-energy unit cell increases. For the centric structure, a decrease of the charges by 40% results in a unit cell length increase of ~ 0.54 Å, while a decrease of charges by 100% involves an increase by ~ 1 Å.

To conclude this section, the structure has been found to be very sensitive to a scaling of the point charges, both with respect to temperatures of conversion from asymmetric to symmetric structure and to the length of the unit cell.

C. Modifications of the rigidity of the lattice

It is interesting at this point to estimate just how dependent the findings are on details of the force field employed. While it may intuitively be easily understandable that the charges in the system should have a strong effect on the unit cell length *vs.* temperature graph, it is far less obvious how or whether a change in force constants of the lattice should affect this representation.

The contributions to potential energy given by bond stretching and bending are given by the set of equations (3).

$$\begin{aligned} U_{ij}(r_{ij}) &= k_r(r_{ij} - r_0)^2 \\ U_{ijk}(\theta_{ijk}) &= k_\theta(\theta_{ijk} - \theta_0)^2 \end{aligned} \tag{3}$$

In the previous section, it was found that over the temperature range 11-423 K no expansion or shrinkage of the unit cell was observed for the model of García–Sánchez et al. In this section, systematic modifications of k_r and k_θ by a factor of 1/2 or 2 were undertaken. In all cases, the frameworks formed had a Δ-parameter of zero. It was further found that the magnitude of k_r governs the absolute value of the unit cell length. A change by a factor two corresponds roughly to an increase of 0.1 Å. Moreover, the simultaneous halving of k_r and doubling of k_θ force

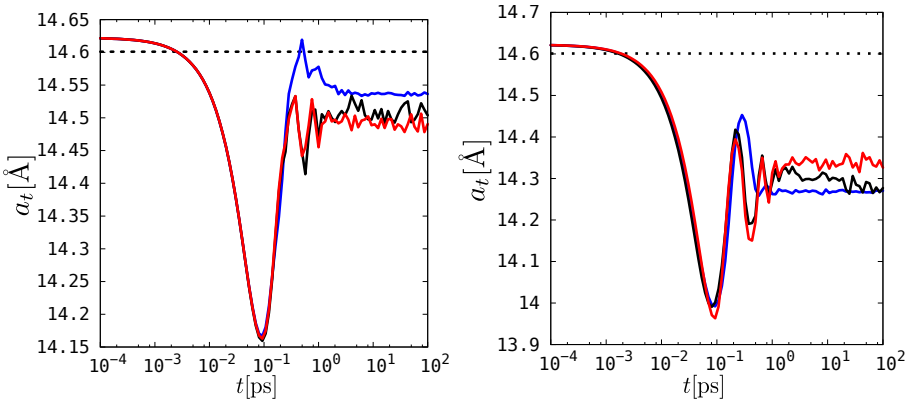

FIG. 8. Length of unit cell a *versus* time t using $k_r \to 2k_r$ and $k_\theta \to \frac{k_\theta}{2}$ (**left**) and $k_r \to \frac{k_r}{2}$ and $k_\theta \to 2k_\theta$ (**right**) at 11 K (blue), 295 K (black), and 423 K (red).

constants led to a positive thermal expansion, while on the contrary a doubling of k_r and halving of k_θ led to a negative thermal expansion. This opens up the possibility in the development of a force field, of tuning the force constants to reproduce known thermal expansions

D. Other potentials

While in previous sections the model of Nicholas and modifications of this model have been investigated, in this section other popular approaches were tested. Probably the simplest force field one can imagine was proposed by Demontis et al.[10]. This force field is not stable in NPT-ensemble calculations, possibly due to the lack of Van der Waals and charge-charge long-range interactions. Oscillations and vibrations in the equilibrium introduce asymmetries in the structure, the lack of charges hinder their disappearance. This potential worked well in a number of applications in the NVT-ensemble in which it was developed, but folded unrealistically due to the lack of torsional, charges and other terms to restrain the movement of the atoms.

Similar graphics to Figure 5 can be constructed for the model by Hill and Sauer[9] and a further refinement of the latter that includes a core shell.[11]

The results are shown in Figure 9 (top and bottom, respectively). Unit cell lengths at roughly 15 Å are in better agreement to experiment than Nicholas et al's model. However, as energy minimizations show, both the symmetric and asymmetric structure converge towards the same minimum and present no secondary minima. Hill and Sauer's model contains strong torsional force constants capable of maintaining the structure. Schröder and Sauer's model on the other side, based on a consistent force field, adapts a core shell to it. Normally, the fixed high symmetry in the structures tends to cancel out any small variation in charge.[7] But, if the volume and geometry of the unit cell are not fixed, the incidence of charges on the symmetry of the lattice is marked.

The simulations with Schröder and Sauer's core shell model increased the degrees of freedom, relaxing the system and thereby resulting in more realistic electrostatic interactions.

Figure 9-b, 9-d, and the corresponding representations in Figures 5 and 7 all show a downwards curvature in the ellipticity *vs.* unit cell length that is matched by the experiment. This behaviour that appears to be fairly universal is probably best understood in the context of flexing mechanically a structure with essentially rigid bond lengths gradually from a distorted geometry ($I\bar{4}3m$ space group) towards a higher-symmetry geometry ($Im\bar{3}m$ space group). It is the potential energy analysis discussed previously (Figures 9-a and 9-c) and the applied external pressure that determine ultimately how inevitable a falling back to the high symmetry model is.

IV. CONCLUSIONS

Structural changes in zeolite RHO between $I\bar{4}3m$ and $Im\bar{3}m$ space groups lead to a change in unit cell length. For this reason, flexible force fields for zeolites are worthwhile studying when the volume is not fixed.

In this work, it was found that the aluminium distribution does not seem to be the primary cause for the structural changes in flexible zeolite RHO. All framework models are unable to reproduce correctly the structural phase transition

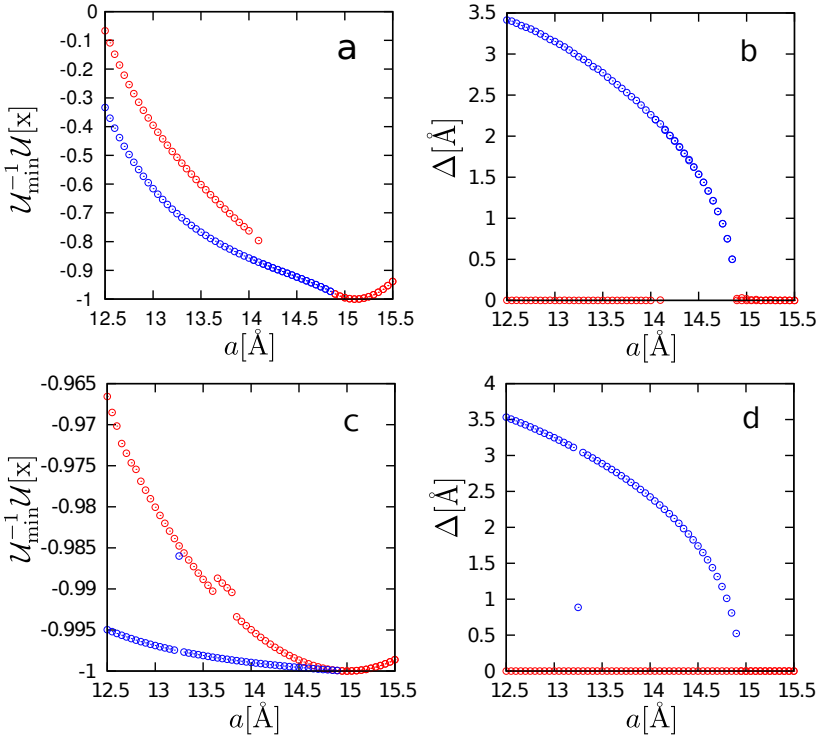

FIG. 9. Equilibrium paths on the potential energy surface $u = -\mathcal{U}_{\min}^{-1}\mathcal{U}(a, \Delta)$ for (a,b in plot) for Hill and Sauer's force field,[8, 9] with $k_B^{-1}\mathcal{U}_{\min} = -1.077 \times 10^6$ K and (c,d in plot) for a core-shell model,[11] with $k_B^{-1}\mathcal{U}_{\min} = -7.25 \times 10^7$ K. Systems with $\Delta < 0.5$ Å in red and $\Delta \geq 0.5$ Å in blue.

with use of energy minimization and molecular dynamics techniques for the isothermal–isobaric ensemble. Energy minimization results were consistent with molecular dynamics simulations.

However, a series of important conclusions could be drawn. Nicholas et al's model was shown by X-ray diffraction and by recording the degree of ellipticity to reproduce the structural changes within the framework. The latter indicator correlates very well with changes in unit cell length in the exact way found experimentally. The main drawback of Nicholas' model consists in too small unit cell lengths. A low volume structure belonging to space group $Pm\bar{3}$ is predicted with this force field as an energetically competitive alternative to high ellipticity structures.

From the point of view of potential energy, decreasing the partial charges in the model reduces the barrier between structural phases and increases the volume of the unit cell. In this way, the study of modifications in the charges of the Nicholas model, in section III-B, and the simulations with Demontis model in section III-D, for the isothermal–isobaric ensemble, suggest that the role of the charges is notable. The Schröder and Sauer model with a core shell model, and Sauer and Hill model with strong torsions maintained the stability of the structure within NPT simulations, reproduced the experimental cell length well, but failed to account for the existence of $I\bar{4}3m$ symmetry. Thus, the potential of Nicholas predicts for the pure silica zeolite RHO two stable structures ($Im\bar{3}m$ and $I\bar{4}3m$). The other potentials predict a single stable structure ($Im\bar{3}m$) and predict a more realistic length of the unit cell.

Finally, it is worth highlighting the effects of modifying simultaneously the bond stretching and bending parameters in a framework model. These parameters drive the thermal expansion of the framework.

V. ACKNOWLEDGMENTS

Dr. S. Hamad is acknowledged for helpful discussions and support on GULP.[22] This work was supported by the European Research Council through an ERC Staring Grant (ERC_279520) and the Spanish Ministerio de Economía y Competitividad (CTQ2010-16077) and a VIDI Grant (D. Dubbeldam).

VI. SUPPORTING INFORMATION AVAILABLE

This material is available in a separated document.

---

[1] V. Kapko, C. Dawson, M. M. J. Treacy, and M. F. Thorpe, Phys. Chem. Chem. Phys. **12**, 8531 (2010).
[2] D. R. Corbin, L. Abrams, G. A. Jones, M. M. Eddy, W. T. A. Harrison, G. D. Stucky, and D. E. Cox, Journal of the American Chemical Society **112**, 4821 (1990).
[3] J. B. Parise and D. E. Cox, The Journal of Physical Chemistry **88**, 1635 (1984).
[4] J. B. Parise, L. Abrams, T. E. Gier, D. R. Corbin, J. D. Jorgensen, and E. Prince, The Journal of Physical Chemistry **88**, 2303 (1984).
[5] Y. Lee, J. A. Hriljac, T. Vogt, J. B. Parise, M. J. Edmondson, P. A. Anderson, D. R. Corbin, and T. Nagai, Journal of the American Chemical Society **123**, 8418 (2001).
[6] J. B. Parise and E. Prince, Materials Research Bulletin **18**, 841 (1983).
[7] J. B. Nicholas, A. J. Hopfinger, F. R. Trouw, and L. E. Iton, Journal of the American Chemical Society **113**, 4792 (1991).
[8] J. R. Hill and J. Sauer, The Journal of Physical Chemistry **98**, 1238 (1994).
[9] J. R. Hill and J. Sauer, The Journal of Physical Chemistry **99**, 9536 (1995).
[10] P. Demontis, G. B. Suffritti, S. Quartieri, E. S. Fois, and A. Gamba, The Journal of Physical Chemistry **92**, 867 (1988), http://pubs.acs.org/doi/pdf/10.1021/j100315a003.
[11] K.-P. Schröder and J. Sauer, The Journal of Physical Chemistry **100**, 11043 (1996).
[12] R. Bueno-Pérez, S. Calero, D. David, C. O. Ania, J. B. Parra, A. P. Zaderenko, and P. J. Merkling, Journal of Physical Chemistry C **116**, 25797 (2012).
[13] M. Palomino, A. Corma, J. L. Jorda, F. Rey, and S. Valencia, Chem. Commun. **48**, 215 (2012).
[14] M. Parrinello and A. Rahman, Journal of Applied Physics **52**, 7182 (1981).
[15] G. L. Martyna, D. J. Tobias, and M. L. Klein, Journal of Chemical Physics **101**, 4177 (1994).
[16] M. E. Tuckerman, Y. Liu, G. Ciccotti, and G. J. Martyna, Journal of Chemical Physics **115**, 1678 (2001).
[17] M. E. Tuckerman, J. Alejandre, R. López-Rendón, A. L. Jochim, and G. J. Martyna, Journal of Physics A: Mathematical and General **39**, 5629 (2006).
[18] J. Baker, Journal of Computational Chemistry **7**, 385 (1986).
[19] W. Miller, C. W. Smith, D. S. Mackenzie, and K. E. Evans, Journal of Materials Science **44**, 5441 (2009).
[20] T. Carey, A. Corma, F. Rey, C. C. Tang, J. A. Hriljac, and P. A. Anderson, Chem. Commun. **48**, 5829 (2012).
[21] A. García-Sánchez, C. O. Ania, J. B. Parra, D. Dubbeldam, T. J. H. Vlugt, R. Krishna, and S. Calero, The Journal of Physical Chemistry C **113**, 8814 (2009).
[22] J. D. Gale and A. L. Rohl, Molecular Simulation **29**, 291 (2003), http://www.tandfonline.com/doi/pdf/10.1080/0892702031000104887.